Article

Depolymerization of plastics by means of electrified spatiotemporal heating

https://doi.org/10.1038/s41586-023-05845-8

Received: 5 May 2022

Accepted: 15 February 2023

Published online: 19 April 2023

Check for updates

Qi Dong[1,9], Aditya Dilip Lele[2,9], Xinpeng Zhao[1,9], Shuke Li[1,9], Sichao Cheng[3], Yueqing Wang[4], Mingjin Cui[1], Miao Guo[1], Alexandra H. Brozena[1], Ying Lin[2], Tangyuan Li[1], Lin Xu[1], Aileen Qi[1], Ioannis G. Kevrekidis[5,6], Jianguo Mei[7], Xuejun Pan[4], Dongxia Liu[3], Yiguang Ju[2]✉ & Liangbing Hu[1,8]✉

Depolymerization is a promising strategy for recycling waste plastic into constituent monomers for subsequent repolymerization[1]. However, many commodity plastics cannot be selectively depolymerized using conventional thermochemical approaches, as it is difficult to control the reaction progress and pathway. Although catalysts can improve the selectivity, they are susceptible to performance degradation[2]. Here we present a catalyst-free, far-from-equilibrium thermochemical depolymerization method that can generate monomers from commodity plastics (polypropylene (PP) and poly(ethylene terephthalate) (PET)) by means of pyrolysis. This selective depolymerization process is realized by two features: (1) a spatial temperature gradient and (2) a temporal heating profile. The spatial temperature gradient is achieved using a bilayer structure of porous carbon felt, in which the top electrically heated layer generates and conducts heat down to the underlying reactor layer and plastic. The resulting temperature gradient promotes continuous melting, wicking, vaporization and reaction of the plastic as it encounters the increasing temperature traversing the bilayer, enabling a high degree of depolymerization. Meanwhile, pulsing the electrical current through the top heater layer generates a temporal heating profile that features periodic high peak temperatures (for example, about 600 °C) to enable depolymerization, yet the transient heating duration (for example, 0.11 s) can suppress unwanted side reactions. Using this approach, we depolymerized PP and PET to their monomers with yields of about 36% and about 43%, respectively. Overall, this electrified spatiotemporal heating (STH) approach potentially offers a solution to the global plastic waste problem.

There is a large amount of plastic waste ending up in the ocean every year, threatening wildlife and harming biodiversity[3]. Furthermore, microplastics and plastic microfibres have been found in the air and municipal drinking water, posing health and ecological concerns[4]. Common but highly unsustainable methods of removing plastic waste include burning or landfilling, with the former being extremely carbon-heavy and air-polluting, whereas the latter can cause long-term damage to the environment. Alternatively, many thermoplastics can be recycled through mechanical processing into low-end but useful materials[5]. However, mechanical plastic-recycling approaches often suffer from limited product value. To continue using plastics, it is imperative to develop efficient plastic recycling and upcycling strategies to ensure a sustainable future[6].

Recently, thermochemical plastic decomposition has emerged as a promising route for converting plastic waste into value-added chemicals[7–10]. Among the numerous thermochemical plastic-decomposition pathways, selective depolymerization to monomers holds great economic incentive, as the generated monomers can be reused in subsequent polymerization reactions for another product life cycle or as chemical feedstocks for other processes[1]. Although a few plastics that have relatively low ceiling temperatures can be readily depolymerized through conventional thermochemical methods such as pyrolysis (for example, poly(methyl methacrylate) and polystyrene)[11,12], most polyolefins and polyesters cannot be converted to their monomers with high selectivity, as conventional approaches lack precise control of the reaction progress. This is because of the complex physicochemical transformations of reactants and intermediate products (for example, melting, vaporization, decomposition etc.), as well as the severe competing side reactions to the depolymerization pathway during continuous heating of the plastic, which lead to a range of products beyond the monomer (for example, gases, condensable hydrocarbons, aromatics etc.)[2,7,13,14]. To solve this problem, conventional thermochemical processes often

[1]Department of Materials Science and Engineering, University of Maryland, College Park, MD, USA. [2]Department of Mechanical and Aerospace Engineering, Princeton University, Princeton, NJ, USA. [3]Department of Chemical and Biomolecular Engineering, University of Maryland, College Park, MD, USA. [4]Department of Biological Systems Engineering, University of Wisconsin-Madison, Madison, WI, USA. [5]Department of Chemical and Biomolecular Engineering, Johns Hopkins University, Baltimore, MD, USA. [6]Department of Applied Mathematics and Statistics, Johns Hopkins University, Baltimore, MD, USA. [7]Department of Chemistry, Purdue University, West Lafayette, IN, USA. [8]Center for Materials Innovation, University of Maryland, College Park, MD, USA. [9]These authors contributed equally: Qi Dong, Aditya Dilip Lele, Xinpeng Zhao, Shuke Li. ✉e-mail: yju@princeton.edu; binghu@umd.edu

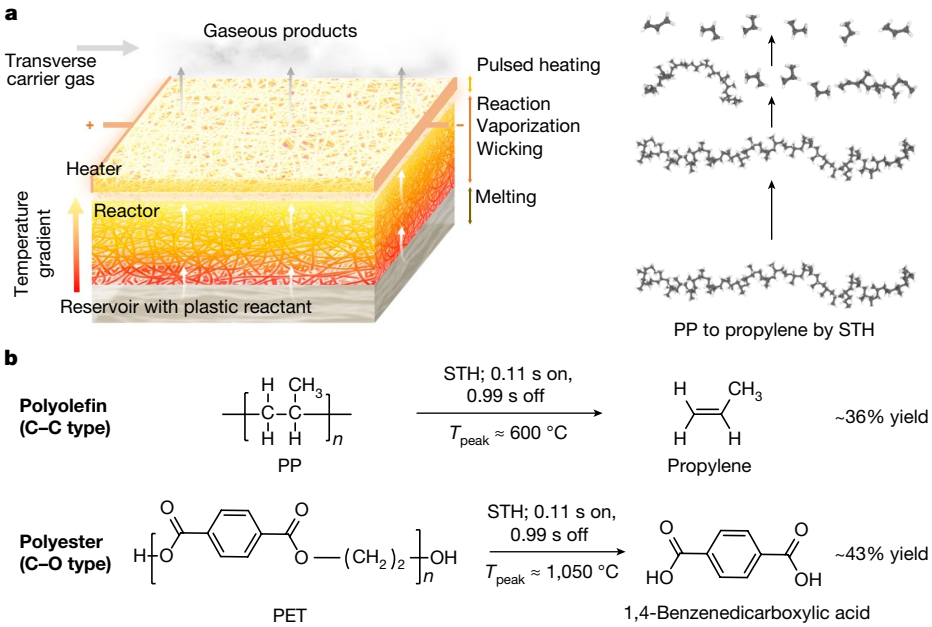

Fig. 1 | The working principle of the electrified STH approach. a, Schematic demonstrating the STH process in the bilayer configuration and the molecular transformation from polymer to monomer using PP as a model plastic. **b**, The depolymerization reactions of PP (as a model polyolefin) and PET (as a model polyester) to their monomers by STH, with yields of about 36% and about 43%, respectively, using a non-optimized pulsed heating programme of 0.11 s power on and 0.99 s power off in every pulse cycle. T_{peak} refers to the peak temperature of the periodic pulse cycles in a temporal heating profile.

use catalysts to enhance the product selectivity. However, catalysts are prone to performance degradation and provide limited improvement of the depolymerization selectivity[5,8]. For example, the pyrolysis of PP typically features a monomer yield of only about 10% without catalysts and <25% using optimized catalysts[15–19]. In another example, the pyrolysis of PET leads to various aromatic species, often with <25% yield to the 1,4-benzenedicarboxylic acid monomer[20–22].

Here we demonstrate a catalyst-free and far-from-equilibrium depolymerization process based on electrified STH, which can control the reaction progress and pathway to convert commodity plastics to monomers with high yields. In this process, a bilayer of porous carbon felt is placed in contact above a reservoir of solid plastic reactant (Fig. 1a). We then apply a pulsed electrical current to the top carbon heater layer, which generates heat that conducts to the bottom carbon reactor layer and the underlying plastic reactant, forming a vertically distributed spatial temperature gradient. This temperature gradient causes the plastic to melt in the reservoir and continuously wick upwards through the porous fibre network of the bottom carbon reactor layer by means of capillary forces (Fig. 1a). Decomposition of the plastic occurs as the liquid polymer experiences sufficiently high temperatures while gradually moving upwards. As the temperature increases, volatile species enter the gas phase (for example, $C_{<20}$ at about 350 °C (ref. [13])), continue to diffuse through the porous structure and interact with higher sections of the reactor layer, as well as the top carbon heater layer for further cracking (Fig. 1a). In these regions, the rapid heating pulses (for example, high heating rate >10^3 °C s^{-1}, T_{peak} up to about 600 °C for PP and about 1,050 °C for PET) provide sufficient energy to break the C–C or C–O bonds that connect the monomer fragments. Meanwhile, the transient heating duration (for example, 0.11 s) in each pulse cycle potentially reduces the energy cost compared with the operation using continuous heating[23] and, more importantly, prevents the reaction from approaching chemical equilibrium that would otherwise result in the formation of a large amount of undesired side products (for example, methane, aromatics)[13,14,24] through random C–C bond breaking, dehydrogenation, C–C bond coupling, aromatization etc. These processes have higher energy requirements and/or longer reaction timescales[25–27], which should be slowed down more intensively compared with the monomer formation process by the rapid cooling (for example, cooling rate >120 °C s^{-1}) after a transient heating duration (for example, 0.11 s) in each pulse cycle, resulting in a high monomer selectivity. Also, the continuous melting, wicking, vaporization and reaction process within the bilayer structure allows the intermediate products (that is, shorter polymers and oligomers in the liquid and gas phases) to gradually diffuse up through the porous scaffold and experience multiplel heating pulses during the increased residence time, thereby reaching a high degree of depolymerization and an improved monomer yield.

Taking advantage of both the spatial and temporal heating effects, we used the electrified STH approach to depolymerize PP and PET as model polyolefin and polyester plastics, respectively, which feature C–C and C–O backbones (Fig. 1b). The yields from polymer to monomer by means of pyrolysis of PP and PET using STH were about 36% and about 43%, respectively, which are considerably higher compared with conventional thermochemical methods[15–22]. Note that our approach does not require any catalysts, as STH not only offers high selectivity by controlling the reaction progress and pathway but also creates periodic high temperatures (for example, about 600 °C every 0.11 s for the pyrolysis of PP) to enable rapid bond activation and thus a high instantaneous reaction rate. We further show that the electrified STH process exhibits good scalability on the laboratory scale and can potentially be operated in a continuous mode using renewable electricity with reduced CO_2 emissions compared with conventional techniques. Overall, this electrified STH process holds great potential for improving the sustainability of commodity plastics.

We first explore this electrified STH approach using PP as a model commodity plastic, as it holds one of the largest market shares among all synthetic polymers[8]. The selective depolymerization of PP to its monomer propylene (C_3H_6) has proved to be challenging owing to the difficulty in controlling the reaction progress and pathway by conventional methods, which often leads to a variety of products of different carbon numbers[15–19,24]. In a typical process, we assembled a STH system by laminating two layers of porous carbon felt (heater layer: 25 × 9 × 2.3 mm; reactor layer: 13 × 6 × 4.7 mm), which were placed on top of a small reservoir that contained the solid PP reactant. This

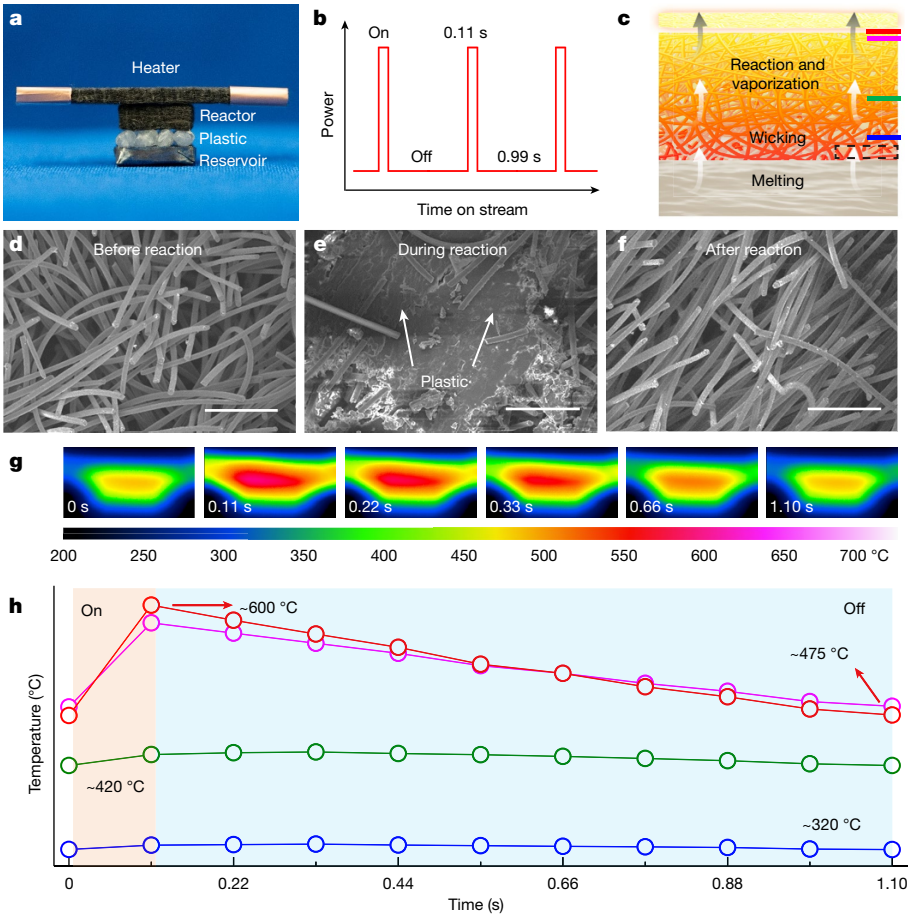

Fig. 2 | The porous carbon felt bilayer of the STH system and its depolymerization process by means of pulsed electrical heating. a, The STH system is assembled from a porous carbon felt 'heater layer' that is placed in soft contact on top of a carbon felt 'reactor layer'. The reactor layer then rests on top of the plastic reactant (PP beads shown here), which is contained within an inert reservoir. Note that in this picture the PP beads are intentionally stacked above rather than inside the reservoir only for demonstrating the assembly of the setup. For STH operations, the PP beads are placed inside the reservoir. For heating, an electric current is passed through the top heater layer by means of the copper electrodes, whereas the bottom reactor layer is non-electrified. **b**, The periodic pulsed electrical signal applied to the STH system. **c**, Schematic of the STH system during pulsed electrical heating. The red, pink, green and blue lines indicate where the temperature profiles were measured for Fig. 2g,h. The dashed black box indicates where the SEM images were taken for Fig. 2d–f. **d**, SEM image showing the bottom region of the pristine reactor layer. **e**, SEM image showing the infiltration of the plastic melt into the bottom region of the reactor layer within 5 min of STH operation (power on for 0.11 s at about 22 V, power off for 0.99 s). **f**, SEM image showing the bottom region of the reactor after 35 min of STH operation. **g**, Temperature maps of the heater and reactor layers at various time points during one heating/cooling cycle of 1.10 s total (power on for 0.11 s at about 22 V, power off for 0.99 s), measured in a lab-built argon-filled environmental chamber. **h**, The temporal temperature profiles at four representative positions of the STH system, in which the red, pink, green and blue curves correspond to the red, pink, green and blue positions shown in **c**. The light-orange region indicates 'power on', whereas the light-blue region indicates 'power off'. Scale bars in **d**–**f**, 100 µm.

structure was housed in a quartz tube (10.5 mm inner diameter) that featured inlet and outlet ports for inert argon carrier gas flow as well as electrical wiring to connect the top carbon heater layer to a power source using Cu electrodes (Fig. 2a and Extended Data Fig. 1; see Methods for details). Applying a repeated electrical pulse to the top carbon heater layer (Fig. 2b) creates a transient Joule heating effect (Extended Data Fig. 1) that we suggest would produce a vertical temperature gradient between the top and bottom surfaces of the reactor layer. The temperature gradient should promote the continuous melting, wicking, vaporization and reaction of the polymer as it moves up through the bilayer carbon felt structure (Fig. 2c). Note that we fabricated the top heater layer using a thinner piece of carbon felt (about 2.3 mm) to reduce the thermal inertia and thereby providing rapid heating and cooling rates, whereas the bottom carbon reactor layer was thicker (about 4.7 mm) to enable gradual wicking of polymer melt and diffusion of volatile intermediate species for an increased residence time.

To demonstrate the STH process, we placed 0.1 g of PP in the reactant reservoir and applied about 22 V to the top heater layer for 0.11 s, followed by 0.99 s of the power turned off. We repeated this electrical pulse cycle for 35 min, at which point all of the PP had reacted from the reservoir. Using scanning electron microscopy (SEM), we observed the wicking of the plastic melt through the bottom of the reactor layer by stopping the batch STH reaction at certain time points. The porous reactor layer is composed of a network of carbon fibres (Fig. 2d), which gradually became filled by the plastic melt within 5 min of pulsed electrical heating (Fig. 2e and Extended Data Fig. 2). After 35 min, the reactor layer once again returned to its original state, with almost no solid residue or solid-phase product observed (Fig. 2f). Also, there was negligible difference in the total weight of the bilayer carbon felts and reservoir before the loading of PP and after 35 min of the batch STH reaction. These results indicate the complete pyrolysis of the plastic and insubstantial coke formation through the applied pulsed electrical heating. Note that the fibres in the carbon felt do not need to be loaded with catalysts to conduct the reaction (although some catalytic residues may remain from the plastic reactant in the previous polymerization processes). This makes the electrified STH approach

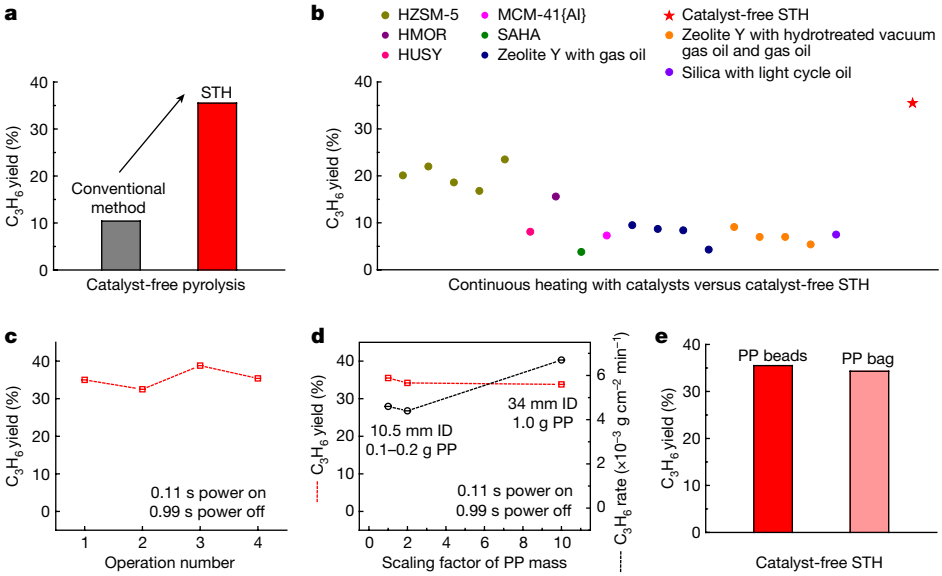

Fig. 3 | The depolymerization performance of the STH approach using PP as a model plastic. a, Comparison of the C_3H_6 monomer yield between our work using STH under far-from-equilibrium conditions and a literature report using catalyst-free pyrolysis by furnace heating under near-equilibrium conditions[18]. **b**, Comparison of the C_3H_6 monomer yield between our work using STH and literature reports using different catalysts, reaction media and/or processes[15–19]. **c**, The C_3H_6 monomer yield of four consecutive PP pyrolysis batch reactions using STH. **d**, The C_3H_6 monomer yield and production rate as a function of the reaction scale. The scaling factor is based on the PP mass feed, with the initial scale of 0.1 g PP defined as 1. **e**, The C_3H_6 monomer yield by STH using PP beads and a commercial PP bag. All STH processes used a programme of 0.11 s on, 0.99 s off and $T_{peak} \approx 600$ °C. The data shown in this figure are listed in Supplementary Tables 1 and 2. ID, inner diameter.

unsusceptible to catalyst degradation, enabling the durability and reusability of the system.

To understand the heating process, we used an infrared camera to measure the temperature distribution at the outer surface of the two carbon felt layers. As the quartz tube wall blocks the infrared signal, we mimicked the configuration of the STH system by placing the bilayer structure in an argon-filled lab-built environmental chamber with an opening to allow the infrared signal to transmit to the infrared camera (see Methods for details). On the basis of the temperature distribution maps acquired with the environmental chamber (Fig. 2g), we extracted four temperature profiles at representative vertical positions (labelled in Fig. 2c) of the bilayer structure within a period of 1.10 s (that is, one pulse cycle, power on for 0.11 s at about 22 V, power off for 0.99 s; Fig. 2h). The interfacial region between the heater and reactor layers seems to have the highest peak temperature (T_{peak}). After turning the power on for 0.11 s, the temperature in this region (red trace, Fig. 2h) quickly rises to about 600 °C then drops back to about 475 °C within 0.99 s after removing the power input to complete the power on/off cycle, corresponding to a heating rate of $>10^3$ °C s^{-1} and a cooling rate of about 126 °C s^{-1}. Note that the temperature ranges at the interfacial region between the heater and reactor layers (red trace) and at the top section of the reactor layer (pink trace) are much higher than the temperature (about 420 °C) at which PP starts to show apparent weight loss (Supplementary Discussion 1), suggesting that the polymer vaporization and reaction processes readily occur below these regions. Unlike these top sections, the middle and bottom sections (green and blue traces) of the reactor layer exhibit much milder temperature variation (<35 °C) within one power on/off cycle, probably because the top section of the reactor layer absorbs most of the radiative heat flux from the heater. These results indicate that the reactants near the top regions of the reactor layer and in the heater layer are subjected to pulsed heating, whereas those near the bottom of the reactor undergo almost continuous heating at nearly constant temperatures. These four temperature profiles also demonstrate a vertically distributed temperature gradient from 475 to 600 °C (top) to about 320 °C (bottom). Note that this temperature measurement setup using an environmental chamber offers better spatial resolution to differentiate the heater and reactor layers; however, the surrounding environment of the carbon felt bilayer (that is, the walls of the environmental chamber) is slightly different from that in the quartz tube used for the real STH operation. To corroborate the environmental-chamber measurements, we also measured the temperature of the bilayer using a customized quartz tube (10.5 mm inner diameter) with a smaller opening on the tube wall for transmitting the infrared signal, which should provide better consistency with the real STH system, although at lower spatial resolution owing to the limited opening size on the tube wall (Extended Data Fig. 3a). The measurement using the customized quartz tube shows almost identical temporal temperature profiles to those shown in Fig. 2h, suggesting the accuracy and robustness of the lab-built environmental chamber for conducting the temperature measurements (Extended Data Fig. 3b,c).

Note that the role played by the bilayer structure is critical for STH as it creates the temperature gradient that ensures a continuous melting, wicking, vaporization and reaction process. If instead of a heater/reactor bilayer design we were to use a single carbon layer to heat the entire plastic melt in the container, there would be no temperature gradient to promote the wicking effect, resulting in poor control of the reaction progress (Supplementary Discussion 2). Also, the gradual wicking and diffusion of the reactants through the porous reactor layer allow the intermediate products to have increased residence times and thereby experience more heating pulses compared with the operation using a single heater layer, which should improve the degree of depolymerization and the monomer yield.

We used gas chromatography with flame ionization detection (GC-FID) to quantify the yield of various species (for example, CH_4, C_2H_4, C_3H_6 etc.) in the argon carrier gas collected downstream during the PP pyrolysis batch reaction (Extended Data Fig. 4). After applying a typical pulsed heating programme (power on for 0.11 s at about 22 V, power off for 0.99 s, one power on/off cycle for 1.10 s; total operation time 35 min) to 0.1 g of PP beads, we achieved a high C_3H_6 monomer yield of 35.5% ± 6.2% (Fig. 3a and Supplementary Table 1), with most of the C_3H_6 monomer obtained in the first 10 min. This yield by the catalyst-free STH process, despite being non-optimized, is already

much higher compared with values reported in the literature through catalyst-free pyrolysis of PP[18] (for example, about 10%; Fig. 3a). Also, the C_3H_6 monomer yield by STH is among the highest compared with the literature even using optimized catalysts and processes, including fast pyrolysis methods that can reduce side reactions by controlling timescales in seconds[15–19] (typically <25%; Fig. 3b and Supplementary Table 1). Note that, compared with such fast pyrolysis methods, our STH approach adds a new dimension of tunability, featuring transient heating durations of milliseconds provided by the heater, which can potentially be combined with existing fast pyrolysis techniques towards even more favourable synthesis outcomes[7,28].

To explore the reaction pathway of the PP pyrolysis and understand the role played by STH, we performed reactive molecular dynamics by ReaxFF, which simulated a spatially and temporally homogeneous reactor[29,30]. The simulation of the reaction process from the starting polymeric molecules to the near-equilibrium products was conducted at 1,527 °C, which was selected to be higher than the operation temperature of STH to extract the complete reaction progress within a reasonable simulation time (that is, <1 year)[31,32]. Extended Data Fig. 5a–d shows a series of representative zoomed-in images of the simulated space to demonstrate the molecular-level transformation of the polymer as it is heated over time (from 0 to around 100 ns). The PP molecules first crack into smaller polymeric species, oligomers, and monomer fragments (at roughly 5.5 ns), which then dehydrogenate, recombine, and gradually form larger and unsaturated species (at about 28 ns and about 100 ns). We plotted the number of monomers as a function of the simulated reaction time (up to about 100 ns) and found that the number quickly peaks at approximately 5.5 ns, then continues to decrease over time (Extended Data Fig. 5e). Meanwhile, the number of H_2 molecules increases throughout the simulated reaction time frame, indicating that the dehydrogenation side reaction (C–H bond breaking) occurs continuously. These results indicate that a transient heating duration (the closer to the timescale of the highest monomer number the better) by the temporal heating profile is useful in terms of achieving high monomer selectivity while reducing side products (for example, methane, aromatics and so on)[13,14,24] whose formation processes have longer timescales. Note that, although continuous heating with long timescales could lead to unwanted side reactions, long residence times are found to promote the formation of gaseous products including the desired monomer (for example, methane, ethylene, acetylene, C_3H_6 monomers) from plastic pyrolysis owing to the increased degrees of depolymerization and cracking[13,28,33,34]. Therefore, the bilayer design with a spatial temperature gradient is critical in terms of exerting increased residence times and thus multiple heating pulses to the reactant and intermediate products by means of a gradual melting, wicking, vaporization and reaction process to improve the monomer yield, meanwhile allowing the temporal heating profile to help reduce side reactions in each heating/cooling cycle.

Increasing the heating rate is also known to improve the plastic pyrolysis yield to gaseous products, including monomers[13,28]. Given that the heating rate of the STH carbon heater is much higher than in conventional devices (for example, >10^3 °C s^{-1} versus 0.33 °C s^{-1} (ref. [18])), we conducted a control experiment to isolate the effect of the heating rate by placing a single carbon heater layer beneath a reservoir containing 0.1 g of PP beads. This setup allowed us to remove both the spatial temperature gradient as well as the temporal heating profile, and focus solely on the impact of the heating rate. With rapid temperature ramping (>10^3 °C s^{-1}, that same as in the STH process) followed by an isothermal hold (that is, continuous heating) at 600 °C (equal to the highest T_{peak} in STH) for 35 min, we obtained a C_3H_6 monomer yield of just 16.7% ± 6%. This result suggests that the fast heating rate by STH has a relatively minor role on the improvement of the monomer yield compared with the spatial temperature gradient and the temporal heating profile.

Next we explored the practicality of the STH approach. We found that the STH system demonstrates good reusability over consecutive operations with consistently high C_3H_6 monomer yields close to 36% (Fig. 3c). We then studied the scalability of the STH approach on the laboratory scale to investigate its potential for practical depolymerization of plastics. As the STH reaction requires a vertical temperature gradient, which confines the potential thickness of the heater and reactor layers, scaling the STH process should depend more on the surface area (that is, width × length) of the bilayers than their volume. Therefore, to scale the reaction, we first increased both the mass of the PP feed and the surface area of the bilayer structure twofold (PP: 0.2 g; heater: 50 × 9 × 2.3 mm; reactor: 26 × 6 × 4.7 mm; Supplementary Table 3), as well as the power input (from about 22 V to about 32 V) to obtain a comparable temperature profile (for example, T_{peak}, heating and cooling durations). The resulting C_3H_6 monomer yield was 34.2%—comparable with the yield measured at the initial scale of 0.1 g PP feed (Fig. 3d). The average C_3H_6 production rates were also comparable at these two scales (that is, 4.6×10^{-3} g cm^{-2} min^{-1} and 4.4×10^{-3} g cm^{-2} min^{-1} for 0.1 g and 0.2 g of PP feed, respectively; Fig. 3d), with most of the C_3H_6 monomers obtained in the first 10 min during the 35-min batch reactions. To further scale up the process, we then fabricated a larger STH system (Extended Data Fig. 6), in which the heater and reactor layers were housed in a larger quartz tube of 34 mm inner diameter, translating to a more than ten times larger cross-sectional area compared with that of the smaller-scale reaction system (Supplementary Table 3), enabling a corresponding increase of the PP feed up to tenfold (from 0.1 g to 1.0 g). With this system and by increasing the surface area of the heater and reactor layers, as well as the applied voltage to maintain the temperature profile (heater layer: 100 × 18 × 2.3 mm; reactor layer: 35 × 12 × 4.7 mm; 40 V), we were still able to obtain a high C_3H_6 monomer yield of 33.8%, which is comparable with the values measured using the smaller-scale STH system (Fig. 3d). The PP was also fully reacted after 35 min, with most of the C_3H_6 monomer detected in the first 12 min. Notably, the average C_3H_6 production rate increased from 4.4–4.6 × 10^{-3} g cm^{-2} min^{-1} to 6.7 × 10^{-3} g cm^{-2} min^{-1} by increasing the size of the quartz tube. This is probably because of the reduced surface area to volume ratio of the larger quartz tube, which improves heat transfer and reduces heat loss of the system. Overall, these results showcase the potential of scaling up the STH approach for practical applications. Last, to demonstrate the utility of this STH approach for commodity plastics, we conducted the pyrolysis of a commercial PP-based product (that is, a PP bag) by applying a typical pulsed heating programme (power on for 0.11 s at about 22 V, power off for 0.99 s, one power on/off cycle for 1.10 s; total operation time: 35 min) with the smaller-scale STH system. Despite having additives such as plasticizers, antioxidants, stabilizers etc. in the PP bag, we still achieved a high C_3H_6 monomer yield of 34.3% ± 7.5% (Fig. 3e), comparable with that from the pyrolysis of PP beads using STH under identical operation conditions (35.5% ± 6.2%).

As well as depolymerizing PP as a representative polyolefin, we also applied the electrified STH approach to depolymerize PET as a representative polyester, which has been widely used as plastics but also as fabrics[8]. To depolymerize PET, we used the STH system to apply a higher T_{peak} compared with PP, given the higher melting point of PET (about 250 °C versus about 160 °C for PP). As a non-optimized, proof-of-concept demonstration, we used a power on (heating) duration of 0.11 s at about 26 V and a power off (cooling) duration of 0.99 s applied to the top carbon heater layer to generate the highest T_{peak} of about 1,050 °C throughout the bilayer structure (Extended Data Fig. 7). By increasing the temperature of the heater, the temperature at the bottom of the reactor increases accordingly, which helps ensure good fluidity of the reactant for effective and continuous wicking through the bottom porous carbon reactor layer. Our qualitative product analysis of the depolymerized PET by gas chromatography–mass spectrometry (GC-MS; Extended Data Fig. 8 and Supplementary Table 4) showed a monomer yield (that is, relative abundance of 1,4-benzenedicarboxylic acid) of up to about 43%, along with roughly 6% monomer-like product

(that is, relative abundance of 1,4-benzenedicarboxylic acid, 1-ethenyl ester), for a total of about 49%. This monomer yield is among the highest compared with the literature of conventional thermochemical methods such as pyrolysis (for example, <25%)[20–22]. The monomer of 1,4-benzenedicarboxylic acid is probably formed on the basis of a β-CH hydrogen transfer mechanism[35] during PET pyrolysis in inert environments, which is supported by the presence of 1,4-benzenedicarboxylic acid, 1-ethenyl ester in the liquid-phase products (Supplementary Table 4) and acetylene in the gas-phase products (Extended Data Fig. 9). Similarly, when we applied the same process to a commercial PET plastic bottle, we obtained a roughly 45% total yield of 1,4-benzenedicarboxylic acid and 1,4-benzenedicarboxylic acid, 1-ethenyl ester, which is close to the approximately 49% total yield of the monomer and monomer-like species from the PET pellets under the same operation conditions.

Besides the broad reactant scope (that is, polyolefins and polyesters) and improved monomer yield, the STH approach also features good potential for continuous processing instead of being conducted in batch reactions. For example, Extended Data Fig. 10 shows a proposed prototype for a plastic depolymerization process based on the same STH bilayer design along with commercially available tools. In this process, solid plastic waste would be mechanically shredded into smaller pieces, which are easier to melt. These pieces would then be dropped into a reservoir kept above the melting temperature to form a liquid. The plastic melt would then fill the reservoir, come into contact with the reactor layer of the bilayer structure and undergo the depolymerization process to produce monomers with high selectivity and yield. Finally, the products would be collected above the bilayer region for further separation and storage. We note that the carbon heater in the STH system can be powered by renewable electricity, whereas the melting of plastic waste can potentially be achieved using renewable energy sources, such as concentrated solar light, making the whole system more energy-efficient, environmentally benign and sustainable with reduced CO_2 emissions.

Conclusion and discussion

In this work, we demonstrate a catalyst-free and far-from-equilibrium electrified STH approach that can selectively depolymerize representative commodity polyolefins (PP) and polyesters (PET) to their monomers at high yields by means of pyrolysis, which offers a promising route for recycling plastic waste. Using a bilayer porous carbon felt structure, we implement a continuous plastic melting, wicking, vaporization and reaction process through pulsed electrical heating. The resulting spatial temperature gradient in the bilayer structure enables a high degree of depolymerization by implementing long residence times on the reactant and intermediates. Meanwhile, the temporal heating profile potentially suppresses the formation of side products and secondary reactions by applying a short heating duration (that is, 0.11 s) in every pulse cycle. We also explored the scalability of the STH approach on the laboratory scale by increasing the surface area of the bilayer, which allowed us to increase the PP mass feed tenfold without compromising the monomer yield, showing the potential of this approach for practical applications.

Note that the monomer yield of the PP and PET pyrolysis reactions by STH described here has not been optimized. To further improve the reaction outcome, the material properties of the reactor layer (for example, pore shape, pore size and distribution, surface energy etc.) could be modified to enhance the plastic melt wicking and gas diffusion processes. Furthermore, unlike continuous heating, the electrified STH process can be controlled by varying the input power and the on/off timescale in milliseconds, enabling us to tune the heating duration, frequency and heating pulse temperature, as well as the temperature distribution in the reactor layer, to optimize the product yield and reduce the energy cost. As we move beyond lab-scale and proof-of-concept demonstrations towards truly large-scale and continuous reactors, data-driven machine learning algorithms (for example, Bayesian optimization of the temperature profile) can also help determine the reaction parameters to optimize the yield tailored to a particular feedstock and desired product[36]. As well as its good performance and potentially better tunability compared with conventional thermochemical methods, the electrified STH approach could be further integrated with commercially available tools for continuous operation using renewable energy sources for higher energy efficiency and reduced CO_2 emissions[37]. Overall, this electrified STH approach holds great potential for converting a range of plastics, biomass and other supramolecules towards the sustainable, energy-efficient and scalable manufacturing of value-added chemicals.

Online content

Any methods, additional references, Nature Portfolio reporting summaries, source data, extended data, supplementary information, acknowledgements, peer review information; details of author contributions and competing interests; and statements of data and code availability are available at https://doi.org/10.1038/s41586-023-05845-8.

1. Häußler, M., Eck, M., Rothauer, D. & Mecking, S. Closed-loop recycling of polyethylene-like materials. *Nature* **590**, 423–427 (2021).
2. Sharuddin, S. D. A., Abnisa, F., Daud, W. M. A. W. & Aroua, M. K. A review on pyrolysis of plastic wastes. *Energy Convers. Manag.* **115**, 308–326 (2016).
3. Jambeck, J. R. et al. Plastic waste inputs from land into the ocean. *Science* **347**, 768–771 (2015).
4. Falco, F. D., Cocca, M., Avella, M. & Thompson, R. C. Microfiber release to water, via laundering, and to air, via everyday use: a comparison between polyester clothing with differing textile parameters. *Environ. Sci. Technol.* **54**, 3288–3296 (2020).
5. Ragaert, K., Delva, L. & Geem, K. V. Mechanical and chemical recycling of solid plastic waste. *Waste Manage.* **69**, 24–58 (2017).
6. Korley, L. T. J., Epps, T. H., Helms, B. A. & Ryan, A. J. Toward polymer upcycling—adding value and tackling circularity. *Science* **373**, 66–69 (2021).
7. Williams, E. A. & Williams, P. T. Analysis of products derived from the fast pyrolysis of plastic waste. *J. Anal. Appl. Pyrolysis* **40**, 347–363 (1997).
8. Ellis, L. D. et al. Chemical and biological catalysis for plastics recycling and upcycling. *Nat. Catal.* **4**, 539–556 (2021).
9. Liu, S., Kots, P. A., Vance, B. C., Danielson, A. & Vlachos, D. G. Plastic waste to fuels by hydrocracking at mild conditions. *Sci. Adv.* **7**, eabf8283 (2021).
10. Algozeeb, W. A. et al. Flash graphene from plastic waste. *ACS Nano* **14**, 15595–15604 (2020).
11. Sun, H., Rosenthal, C. & Schmidt, L. D. Oxidative pyrolysis of polystyrene into styrene monomers in an autothermal fixed-bed catalytic reactor. *ChemSusChem* **5**, 1883–1887 (2012).
12. Kaminsky, W. & Franck, J. Monomer recovery by pyrolysis of poly(methyl methacrylate) (PMMA). *J. Anal. Appl. Pyrolysis* **19**, 311–318 (1991).
13. Zolghadr, A. et al. On the method of pulse-heated analysis of solid reactions (PHASR) for polyolefin pyrolysis. *ChemSusChem* **13**, 4214–4227 (2021).
14. Demirbaş, A. Recovery of chemicals and gasoline-range fuels from plastic wastes via pyrolysis. *Energy Sources* **27**, 1313–1319 (2005).
15. Lin, Y.-H. & Sharratt, P. N. Catalytic conversion of polyolefins to chemicals and fuels over various cracking catalysts. *Energy Fuels* **12**, 767–774 (1998).
16. Scotp, D. S., Majerski, P., Piskorz, J., Radlein, D. & Barnickel, M. Production of liquid fuels from waste plastics. *Can. J. Chem. Eng.* **77**, 1021–1027 (1999).
17. Lovás, P., Hudec, P., Jambor, B., Hájeková, E. & Horňáček, M. Catalytic cracking of heavy fractions from the pyrolysis of waste HDPE and PP. *Fuel* **203**, 244–252 (2017).
18. Encinar, J. M. & González, J. F. Pyrolysis of synthetic polymers and plastic wastes. Kinetic study. *Fuel Process. Technol.* **89**, 678–686 (2008).
19. Arandes, J. M., Ereña, J., Azkoiti, M. J., López-Valerio, D. & Bilbao, J. Valorization by thermal cracking over silica of polyolefins dissolved in LCO. *Fuel Process. Technol.* **85**, 125–140 (2004).
20. Dimitrov, N., Krehula, L. K., Siročić, A., & Hrnjak-Murgić, Z. Analysis of recycled PET bottles products by pyrolysis-gas chromatography. *Polym. Degrad. Stab.* **98**, 972–979 (2013).
21. Yoshioka, T., Grause, G., Eger, C., Kaminsky, W. & Okuwaki, A. Pyrolysis of poly(ethylene terephthalate) in a fluidised bed plant. *Polym. Degrad. Stab.* **86**, 499–504 (2004).
22. Jia, H., Ben, H., Luo, Y. & Wang, R. Catalytic fast pyrolysis of poly (ethylene terephthalate) (PET) with zeolite and nickel chloride. *Polymers* **12**, 705 (2020).
23. Dong, Q. et al. Programmable heating and quenching for efficient thermochemical synthesis. *Nature* **605**, 470–476 (2022).
24. Williams, P. T. & Williams, E. Recycling plastic waste by pyrolysis. *J. Energy Inst.* **71**, 81–93 (1998).
25. Huang, J. B., Zeng, G. S., Li, X. S., Cheng, X. C. & Tong, H. Theoretical studies on bond dissociation enthalpies for model compounds of typical plastic polymers. *IOP Conf. Ser. Earth Environ. Sci.* **167**, 012029 (2018).
26. John, P. C. S., Guan, Y., Kim, Y., Kim, S. & Paton, R. S. Prediction of organic homolytic bond dissociation enthalpies at near chemical accuracy with sub-second computational cost. *Nat. Commun.* **11**, 2328 (2020).
27. Marongiu, A., Faravelli, T. & Ranzi, E. Detailed kinetic modeling of the thermal degradation of vinyl polymers. *J. Anal. Appl. Pyrolysis* **78**, 343–362 (2007).

28. Vollmer, I. et al. Beyond mechanical recycling: giving new life to plastic waste. *Angew. Chem. Int. Edn* **59**, 15402–15423 (2020).
29. van Duin, A. C. T., Dasgupta, S., Lorant, F. & Goddard, W. A. ReaxFF: a reactive force field for hydrocarbons. *J. Phys. Chem. A* **105**, 9396–9409 (2001).
30. Chenoweth, K., van Duin, A. C. T. & Goddard, W. A. ReaxFF reactive force field for molecular dynamics simulations of hydrocarbon oxidation. *J. Phys. Chem. A* **112**, 1040–1053 (2008).
31. Chen, T. B. Y. et al. Characterisation of pyrolysis kinetics and detailed gas species formations of engineering polymers via reactive molecular dynamics (ReaxFF). *J. Anal. Appl. Pyrolysis* **153**, 104931 (2021).
32. Lele, A., Kwon, H., Ganeshan, K., Xuan, Y. & Duin, A. C. T. V. ReaxFF molecular dynamics study on pyrolysis of bicyclic compounds for aviation fuel. *Fuel* **297**, 120724 (2021).
33. Gracida-Alvarez, U. R., Orcid, M. K. M., Sacramento-Rivero, J. C. & Shonnard, D. R. Effect of temperature and vapor residence time on the micropyrolysis products of waste high density polyethylene. *Ind. Eng. Chem. Res.* **57**, 1912–1923 (2018).
34. Zhao, D., Wang, X., Miller, J. B. & Huber, G. W. The chemistry and kinetics of polyethylene pyrolysis: a process to produce fuels and chemicals. *ChemSusChem* **13**, 1764–1774 (2020).
35. Montaudo, G., Puglisi, C. & Samperi, F. Primary thermal degradation mechanisms of PET and PBT. *Polym. Degrad. Stab.* **42**, 13–28 (1993).
36. Shields, B. J. et al. Bayesian reaction optimization as a tool for chemical synthesis. *Nature* **590**, 89–96 (2021).
37. Wismann, S. T. et al. Electrified methane reforming: a compact approach to greener industrial hydrogen production. *Science* **364**, 756–759 (2019).

Methods

Materials

PP (isotactic, average M_w about 580,000, average M_n approximately 166,000) and PET (granular) were purchased from Sigma-Aldrich. Commodity plastic products, including PP bags and PET water bottles, were purchased from Amazon. Solvents, including tetrahydrofuran (HPLC grade) and acetone (>99.9%), were purchased from Sigma-Aldrich. Gases including argon, CH_4, C_2H_4 and C_3H_6 (>99.9%) were purchased from Airgas. Carbon felt (AvCarb G280A, AvCarb G475 and AvCarb G650A, soft graphite battery felt) was purchased from the Fuel Cell Store. Before use, the carbon felt was thoroughly washed with acetone and then dried under vacuum overnight at 80 °C. It was further purged in argon atmosphere for 1 h before use to remove any trapped moisture and oxygen in the porous material. Multipurpose 110 copper sheets (99.9%, 0.002 in. thick) and multipurpose 110 copper wire (99.9%, 0.04 in. diameter) were obtained from McMaster-Carr. Alligator clips made of stainless steel were purchased from Amazon. All the materials used as electrical connections were cleaned with acetone and dried under vacuum before assembling the STH system. Alumina ceramic tubes (99.8%, 0.125 in. outer diameter and 0.062 in. inner diameter, maximum temperature 1,950 °C) were acquired from Omega for covering the copper wires. Quartz tubes were purchased from QSI (1/2 in. outer diameter, 10.5 mm inner diameter) and Technical Glass Products, Inc. (39 mm outer diameter, 34 mm inner diameter). The J-B Weld HI-TEMP RTV silicone gasket maker and sealant was purchased from Amazon.

STH operation

The dimensions of the carbon felt heater (exposed region) and reactor and the flow rate of the argon carrier gas are listed in Supplementary Table 3 for various scales. Both ends of the carbon felt heater were wrapped with copper foil, which were then connected to the power supply through alumina-covered copper wires and alligator clips. The gaps between the copper wire and alumina tube were filled with thermoset epoxy (Gorilla). The reactor layer was placed under the heater in soft contact (that is, without external pressure) and placed on top of a reservoir made of inert titanium foil. The reservoir container was used to hold the plastic reactant and the resulting melt during heating. The size of the titanium container matched that of the reactor. Note that, as the temperature of the reservoir during STH operation is much lower than the reaction temperature, according to the infrared camera heat maps (Fig. 2g), negligible chemical reaction will occur in the reservoir. Finally, the assembled STH system, including the heater layer, reactor layer and reactant reservoir, was placed in a flow reaction system made of a quartz tube (1/2 in. outer diameter, 10.5 mm inner diameter for the small-scale reaction system, QSI; or 39 mm outer diameter, 34 mm inner diameter for the larger-scale reaction system, Technical Glass Products, Inc.). For the small-scale reaction system, the quartz tube was sealed with two Ultra-Torr tee fittings (Swagelok). For the larger-scale STH system, the quartz tube was sealed with sealant (J-B Weld HI-TEMP RTV Silicone Gasket Maker and Sealant) and attached to customized stainless-steel fittings (Extended Data Fig. 6). The ports of the Ultra-Torr fittings were used for the electrical wires and gas flow. Control over the temperature was achieved through a solid-state relay device (DC input and DC output, maximum current 25 A, Omega), a high-accuracy sourcemeter (Keithley, Model 2400) and a power supply (75 V, 20 A, Volteq) connected to the top carbon felt heater layer.

The temperature range, heating duration and heating frequency can be programmed by adjusting the settings of the power supply and the sourcemeter. Control experiments under continuous heating were conducted using a constant power input by the power supply, without the need for the sourcemeter and the relay device. In a typical STH operation with electrical pulsed heating, the heating duration can be programmed through the sourcemeter by setting a certain time within one period (for example, 1.10 s) as 'power on' (for example, 0.11 s, power on) by applying the power and setting the remaining time as 'power off' (for example, 0.99 s, power off) by removing the power. The peak temperature was controlled by the power input (that is, the applied voltage to the heater) from the power supply. In a typical experiment, 0.1–1.0 g of PP beads or about 0.2 g of PET pellets were used as the starting material. For PP bags and PET water bottles, the starting materials were cut into small pieces to fit into the reservoir.

Product detection in the gas phase

Gas products were detected and quantitatively measured by GC-FID (Agilent, Model 6890N). The gas sample was collected at the exit of the reaction system using a SupelInert multilayer foil gas sampling bag (0.6 litres for the small-scale STH system and 5.0 litres for the larger-scale STH system; Extended Data Fig. 4, inset). Fifty-microlitre gas samples were then extracted from the gas bag using a gas-tight syringe (50 µl, Hamilton 1705) and injected into the injection ports of the FID. A thermal conductivity detector was used to quantify an internal standard gas (argon) to ensure the consistency of each injection. The column connected to the FID was a GS-GasPro (Agilent). The column connected to the thermal conductivity detector was a ShinCarbon ST packed column (Restek). Standard gases of CH_4, C_2H_4 and C_3H_6 were injected to calibrate the GC-FID peak areas.

Product detection in the liquid phase

Liquid products were detected and qualitatively measured by GC-MS analysis. The depolymerization products in the liquid phase were in part collected with the carrier gas downstream in an acetone-filled vial. The remainder of the products was condensed in the quartz tube, which was rinsed off using acetone and combined with the downstream products. The acetone solution was filtered through a 0.45-µm syringe filter before injecting into the GC-MS. We used a Shimadzu GCMS-QP2010S system with an Rtx-5MS column (30 m × 0.25 mm, length × inner diameter, with 0.25 µm film thickness). The products from PET depolymerization were silylated to improve the sample volatility. In a typical measurement, 400 µl of the sample was mixed and reacted with 100 µl *N*,*O*-bis(trimethylsilyl)trifluoroacetamide (BSTFA) at room temperature overnight. Helium was used as the carrier gas, with a flow rate of 1.27 ml min^{-1}. The GC oven temperature was programmed from 50 °C (5 min) to 150 °C at a heating rate of 10 °C min^{-1}, from 150 °C to 220 °C at 5 °C min^{-1} and from 220 °C to 300 °C (10 min) at 10 °C min^{-1}. The injector temperature was set at 280 °C in split mode, with a split ratio of 5:1. The MS detector was operated in electron impact ionization mode, with the ion source temperature set at 230 °C. The scanning ion range was set between m/z 35 and 600. Qualitative analysis was performed using GCMS Postrun Analysis software. The products were identified on the basis of the NIST08 and NIST08s libraries and the percentages of the peaks were calculated from the total ion chromatogram peak area.

Determining the product yield

For determining the product yield of PP pyrolysis, the GC-FID peak areas of CH_4, C_2H_4 and C_3H_6 (the main gaseous products from PP pyrolysis in this study by either STH or continuous heating) were quantitatively calibrated by injecting known amounts of standard gases. On the basis of the measured peak areas, the mass of each gaseous product from a batch reaction can be derived. The product yield is then calculated by dividing the mass of the product of interest by the feed mass of PP. Standard deviation is calculated with a value of $n \geq 3$.

The product yield (that is, relative abundance) of PET pyrolysis was qualitatively estimated on the basis of the GC-MS peak area percentages of the liquid-phase products after 55 min of reaction. This method follows the common practice in the literature when quantifying a specific product in a complex mixture[38,39]. Note that minimal solid (<1%) or gaseous products (<5%) were detected after the PET pyrolysis by STH. About 0.2 g of PET can be fully decomposed after 55 min (that is, approximately 100% conversion).

Determining the average C_3H_6 production rate

The average C_3H_6 production rate was calculated by dividing the produced mass of C_3H_6 by the surface area of the reactor layer and the reaction time used to collect the C_3H_6 product during the batch reactions. Note that the C_3H_6 production rate changes over time. The values shown in Fig. 3d are the average reaction rates corresponding to the time used to collect most of the C_3H_6 product for all scales (that is, 10 min for a scaling factor of 1 or 2 and 12 min for a scaling factor of 10).

Temperature acquisition

Temperature mapping of the heater and reactor was performed by an infrared camera VarioCAM HDx head 600 (7.5–14 μm) with a resolution of 640 × 480 infrared pixels using a standard lens (20 mm). The VarioCAM camera has an infrared image rate of 30 Hz in full frame and can measure the temperature in the range −40–1,700 °C with an accuracy of ±2%. During the measurement, the VarioCAM camera was place 10 cm away from the heater and reactor.

To estimate the temporal temperature profile, we first built a homemade model setup to mimic the real STH system, which was housed in an environmental chamber (23 × 13 × 8 cm) composed of thin aluminium siding and a side opening (10 × 4 cm) for the infrared signal to pass through to the camera. The chamber was continuously purged with argon to remove air through one inlet and outlet. We placed the carbon felt bilayer structure along with the PP reactant inside the environmental chamber, applied the same electrical signal used in the real STH system and measured the temperature profile. This result is shown in Fig. 2g,h, as it features good spatial resolution to differentiate the heater and reactor layers.

To acquire potentially better temperature accuracy, the temporal temperature profile of the bilayer structure during STH operation was also measured by the infrared camera using a customized quartz tube with a smaller opening on the tube wall (about 7 × 14 mm), which was created to allow the infrared signal to pass through to the camera. Argon protecting gas was purged to the surrounding environment to avoid air leaking into the quartz tube. We placed the bilayer structure with the PP reactant inside the customized quartz tube, applied the same electrical signal used in the real STH system and measured the temperature profile, the results of which are shown in Extended Data Fig. 3. This setup offers better temperature-measurement accuracy because it best resembles the real STH system, except for the small opening on the side of the quartz tube. However, this small opening and the background noise produced by the quartz tube reduces the spatial resolution for differentiating the position of the heater and reactor layers.

Note that both measurements were conducted in a relatively open space (quartz tube with a small opening or in the environmental chamber with a large opening) rather than in a closed quartz tube as in the real STH operation, therefore it is necessary to estimate the error caused by this factor. To do so, we further measured the temperature of the outer surface of the quartz tube (1/2 in. outer diameter, 10.5 mm inner diameter, QSI) during real STH operations (0.11 s power on, 0.99 s power off, about 22 V). The outer surface of the quartz tube showed a nearly constant temperature of about 145 °C. Because the heating programme and power input to the carbon heater and reactor layers in the quartz tube with a small opening or in the environmental chamber are the same as those in the intact quartz tube, assuming that the energy loss to the surroundings in the real STH system is equal to that in the systems used for the temperature measurement, the measured surface temperature of the carbon heater and reactor layers can be roughly corrected as:

$$T_C = \sqrt[4]{T_M^4 - T_{ambient}^4 + T_{tube}^4}$$

in which T_C and T_M are the corrected and measured surface temperatures of the carbon heater and reactor layers in the quartz tube with the small opening, respectively, and $T_{ambient}$ and T_{tube} are the ambient temperature (20 °C) and quartz tube temperature (145 °C) during the STH operation. On the basis of this estimate, the error of the temperature measurement should be <24 °C for both setups. Note that this error becomes smaller at higher temperatures and larger at lower temperatures (for example, error = 6 °C at 700 °C, error = 9 °C at 600 °C, error = 24 °C at 340 °C).

Material characterization

SEM was conducted using a JEOL 6340F microscope operated at an accelerating voltage of 10–20 kV. The SEM images were taken from the selected region shown in Fig. 2c. The SEM image with infiltrated reactants corresponds to the morphology of the bottom region of the reactor layer within 5 min of the STH operation using PP as a model material (0.11 s power on, 0.99 s power off, about 22 V). Thermogravimetric analysis was conducted using a Discovery SDT 650 instrument from room temperature to 1,000 °C in nitrogen, with a ramping rate of 5 °C min^{-1}.

Molecular dynamics simulations

The molecular dynamics simulation results presented in this work were performed at constant amount of substance (N), volume (V) and temperature (T) using ReaxFF[29,30] reactive molecular dynamics code as a part of the LAMMPS software suite[40,41]. The CHON-2019 ReaxFF parameters set[42] was used in this work to perform reactive classical molecular dynamics simulations, which has been previously used in polymer simulations[43–45]. The ReaxFF reactive-force-field-based molecular dynamics is a computational tool for atomistic-scale simulations of complex reactive systems[29,30]. The ReaxFF reactive force field is trained using quantum mechanics data. A bond-order formalism is used to describe reactive events through the ReaxFF potential. This allows ReaxFF to describe bond formation and breaking. ReaxFF can model much larger simulation systems (thousands of atoms) over relatively long simulation times (more than 100 ns in this work) compared with quantum-mechanics-based methods because of its lower computational cost. This makes ReaxFF a suitable tool to model complex reactive systems such as PP pyrolysis. Furthermore, any chemical intuition is not required to determine possible reactions before performing the simulations.

The ReaxFF method uses a bond-order concept[46] to describe reactive events. The bond order is calculated on the basis of the interatomic distance using an expression that contains the single, double and triple bond-order contributions. ReaxFF allows bond formation and bond breaking by updating the bond order at every iteration. van der Waals and Coulomb interactions, which are non-bonded interactions[29,30], are calculated between every atomic pair independently from the bonded interactions. The energy of each atom governs the dynamics of the system by the following equation:

$$E_{system} = E_{bond} + E_{over} + E_{under} + E_{lp} + E_{val} + E_{tor} + E_{vdWaals} + E_{Coulomb}$$

In the above equation, E_{bond} (bond energy), E_{over} (overcoordination penalty energy), E_{under} (undercoordination penalty energy), E_{lp} (lone pair energy), E_{val} (valence angle energy) and E_{tor} (torsion angle energy) are bond-order-dependent terms. $E_{vdWaals}$ (van der Waals energy) and $E_{Coulomb}$ (Coulomb energy) are non-bonded terms. A more detailed description can be found in previous ReaxFF-related literature[29,30]. The principles and applications of the ReaxFF method have also been discussed in recent literature[47].

The CHON-2019 ReaxFF parameters set[42] was used in this work to perform reactive classical molecular dynamics simulations. The overall simulation methodology can be described as follows: first, energy minimization was performed on all the molecular structures. The energy-minimized polymer structures are then used to randomly fill a periodic simulation box. This simulation system is then energy-minimized at 0 K and equilibrated. The equilibration

temperature is chosen such that no reactions were taking place during equilibration. The equilibrated system is then used to perform the final simulations. The Nosé–Hoover thermostat[48] was used to control the simulation temperature. A damping constant of 100 fs was used for the simulation temperature thermostatting. The simulations time step was chosen to be 0.1 fs following previous work[32,49]. A cubic (88.5 × 88.5 × 88.5 Å) simulation box was filled with 20 randomly placed polymers. Each PP polymer was constructed with 40 monomers. The number density of species formed throughout the simulation time was identified to perform the analysis presented in Extended Data Fig. 5, which was performed at 1,527 °C.

We calculated the general uncertainties for these simulations by averaging the results of several simulations. A different initial geometry was used in each of these simulations. Ten periodic simulation boxes randomly filled with 20 PP polymer molecules as described above were used to generate these initial geometries. The average number density of these ten simulations is used to determine the statistical uncertainty of the simulations. The major product number density uncertainty was up to 10%.

Data availability

Data supporting this study are available from the corresponding authors on reasonable request. Source data are provided with this paper.

Code availability

The code used in this study is available from the corresponding authors on reasonable request.

38. Zhao, X. et al. Hydrothermal treatment of e-waste plastics for tertiary recycling: product slate and decomposition mechanisms. *ACS Sustain. Chem. Eng.* **7**, 1464–1473 (2019).
39. Lu, Q. et al. Influence of pyrolysis temperature and time on the cellulose fast pyrolysis products: analytical Py-GC/MS study. *J. Anal. Appl. Pyrolysis* **92**, 430–438 (2011).
40. Aktulga, H. M., Fogarty, J. C., Pandit, S. A. & Grama, A. Y. Parallel reactive molecular dynamics: numerical methods and algorithmic techniques. *Parallel Comput.* **38**, 245–259 (2012).
41. Thompson, A. P. et al. LAMMPS - a flexible simulation tool for particle-based materials modeling at the atomic, meso, and continuum scales. *Comput. Phys. Commun.* **271**, 108171 (2022).
42. Kowalik, M. et al. Atomistic scale analysis of the carbonization process for C/H/O/N-based polymers with the ReaxFF reactive force field. *J. Phys. Chem. B* **123**, 5357–5367 (2019).
43. Mao, Q., Rajabpour, S., Kowalik, M. & van Duin, A. C. T. Predicting cost-effective carbon fiber precursors: unraveling the functionalities of oxygen and nitrogen-containing groups during carbonization from ReaxFF simulations. *Carbon* **159**, 25–36 (2020).
44. Rajabpour, S. et al. Low-temperature carbonization of polyacrylonitrile/graphene carbon fibers: a combined ReaxFF molecular dynamics and experimental study. *Carbon* **174**, 345–356 (2021).
45. Zhang, L. et al. Converting PBO fibers into carbon fibers by ultrafast carbonization. *Carbon* **159**, 432–442 (2020).
46. Johnston, H. S. & Parr, C. Activation energies from bond energies. I. Hydrogen transfer reactions. *J. Am. Chem. Soc.* **85**, 2544–2551 (1963).
47. Senftle, T. P. et al. The ReaxFF reactive force-field: development, applications and future directions. *NPJ Comput. Mater.* **2**, 15011 (2016).
48. Nosé, S. A unified formulation of the constant temperature molecular dynamics methods. *J. Chem. Phys.* **81**, 511–519 (1984).
49. Kwon, H. et al. ReaxFF-based molecular dynamics study of bio-derived polycyclic alkanes as potential alternative jet fuels. *Fuel* **279**, 118548 (2020).

Acknowledgements This work is not directly funded. L.H. acknowledges support from the University of Maryland A. James Clark School of Engineering. Y.J. acknowledges US Department of Energy (DOE) grant support for the Plasma Science Center (DOE DE-SC0020233) and DOE Basic Energy Sciences (BES) grant DE-SC0021135. S.C. and D.L. acknowledge support from the DOE Office of Fossil Energy (DE-FE0031877). J.M. acknowledges the Richard and Judith Wien Professorship for unrestricted support. The authors acknowledge the Maryland NanoCenter, the Surface Analysis Center and the AIM Lab.

Author contributions L.H. and Q.D. conceived the concept and designed the STH approach. L.H. and Q.D. designed the reactors, with input from S.C. and Y.L. Q.D., S.L., M.G., M.C., T.L. and A.Q. collected the experimental data. X.Z. conducted the temperature measurement, with help from Q.D. and S.L. A.D.L. and Y.J. conducted the molecular dynamics simulations. S.C. and D.L. analysed the gaseous products. Y.W. and X.P. analysed the liquid products. I.G.K. and J.M. helped with the data analysis and improved the manuscript. L.X. helped with the writing and figure design. L.H., Q.D. and A.H.B. collectively wrote the paper, with input from all authors. L.H. and Y.J. supervised the project. All authors discussed the results and contributed to the final manuscript.

Competing interests Q.D., S.C., D.L., Y.J. and L.H. report a PCT patent application of 'High temperature, pulsed heating reactor and methods for polymer recycling'.

Additional information

Supplementary information The online version contains supplementary material available at https://doi.org/10.1038/s41586-023-05845-8.

Correspondence and requests for materials should be addressed to Yiguang Ju or Liangbing Hu.

Peer review information *Nature* thanks the anonymous reviewers for their contribution to the peer review of this work.

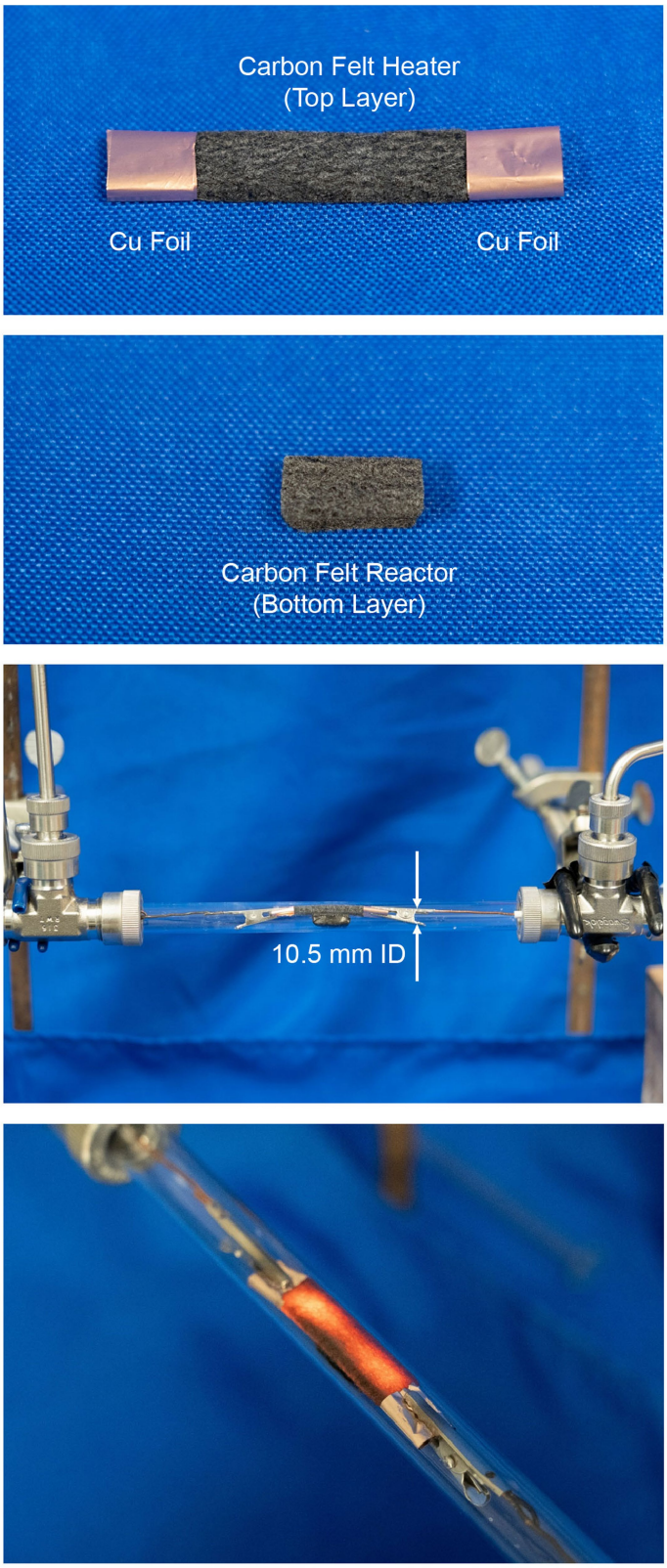

Extended Data Fig. 1 | The assembly of the STH system. A thinner layer of carbon felt (about 2.3 mm) is used as the top heater layer. The two ends of the top heater layer are wrapped with Cu foil electrodes for Joule heating. The top and bottom layers are placed in soft contact (without external pressure) for the STH process. A quartz tube with 10.5 mm inner diameter was used to contain the carbon bilayer structure and the reactant reservoir. The bottom image shows the heater layer exhibiting a bright orange colour as we apply an electrical current through the top heater layer, demonstrating its Joule-heating capabilities.

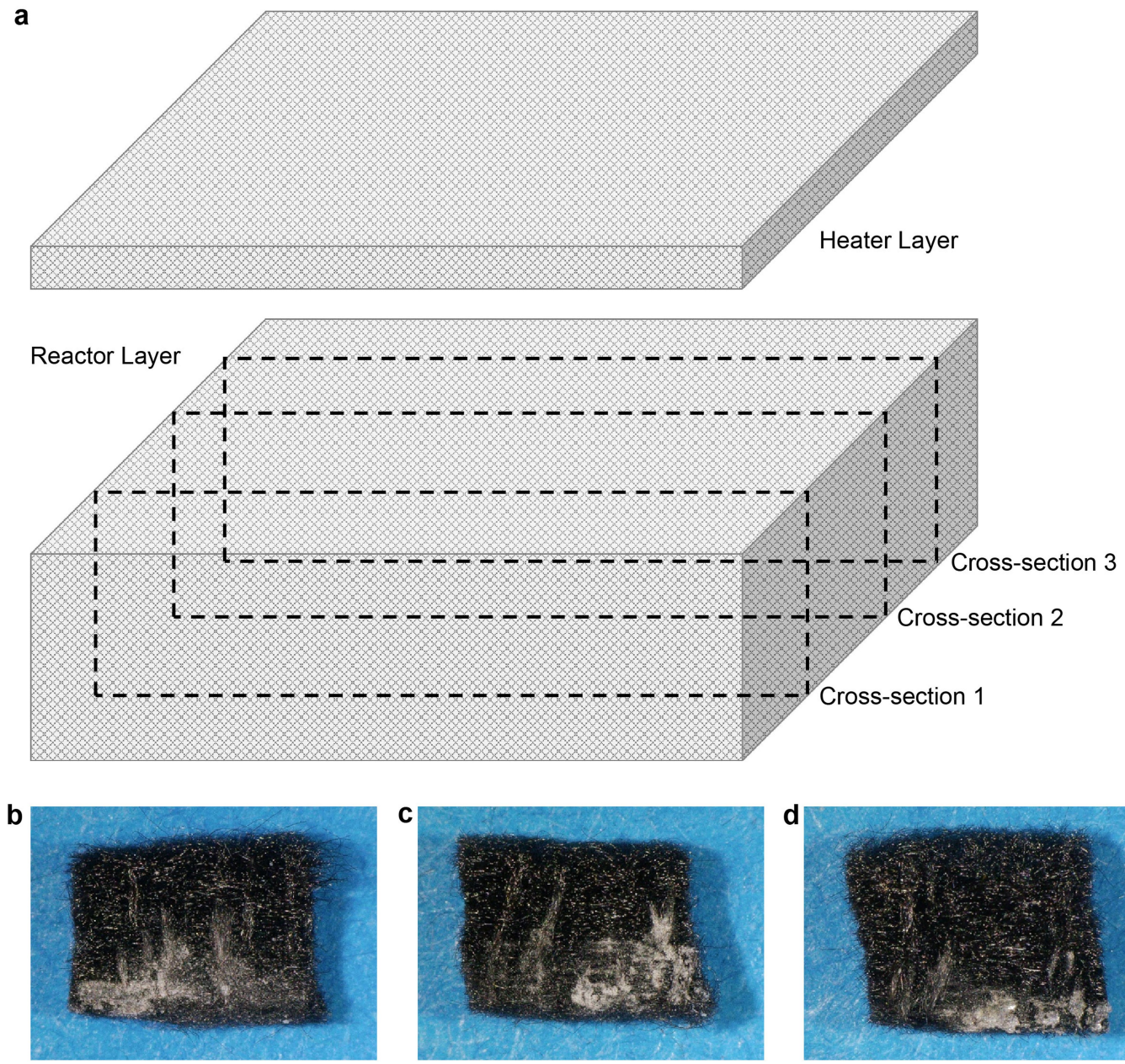

Extended Data Fig. 2 | Characterization of the wicked PP melt. a, Schematic showing the position of the cross-sections cut from the reactor layer after STH operation for about 6 min (0.11 s power on at about 22 V, 0.99 s power off; small-scale reaction system). **b**–**d**, Representative optical microscopy images showing the wicking of PP in the reactor layer. The images correspond to the cross-sections shown in **a**. The white species are wicked plastic melt. The black objects are the cut pieces of the porous reactor layer with cross-sections facing out.

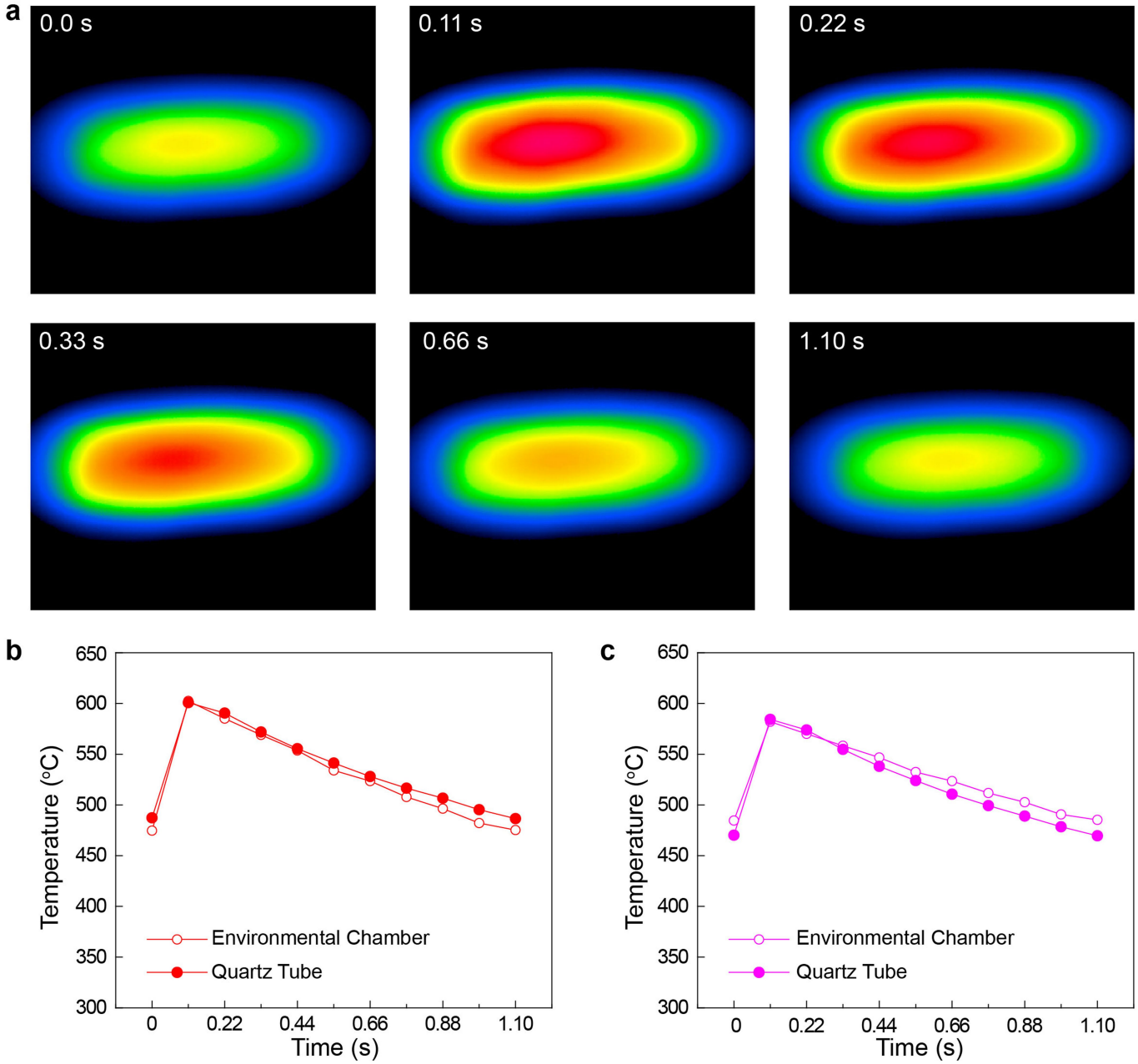

Extended Data Fig. 3 | Temperature measurement using the customized quartz tube with a small opening. a, Temperature maps of the heater and reactor layers at various time points during one heating cycle of 1.10 s (power on time: 0.11 s at about 22 V; power off time: 0.99 s), measured in the customized quartz tube with a small opening (about 7 × 14 mm) on the tube wall. The temperature scale is the same that as shown in Fig. 2g. This temperature measurement features better accuracy, as the bilayer structure is housed in a quartz tube setup similar to the real STH process but has lower spatial resolution because of the limited size of the opening on the quartz tube wall and background noise from the quartz tube for differentiating the position of the heater and reactor layers compared with the measurement using the environmental chamber. **b**, Comparing the temporal temperature profiles measured using the lab-built environmental chamber and the customized quartz tube at the position labelled in red as shown in Fig. 2c. **c**, Comparing the temporal temperature profiles measured using the lab-built environmental chamber and the customized quartz tube at the position labelled in pink as shown in Fig. 2c.

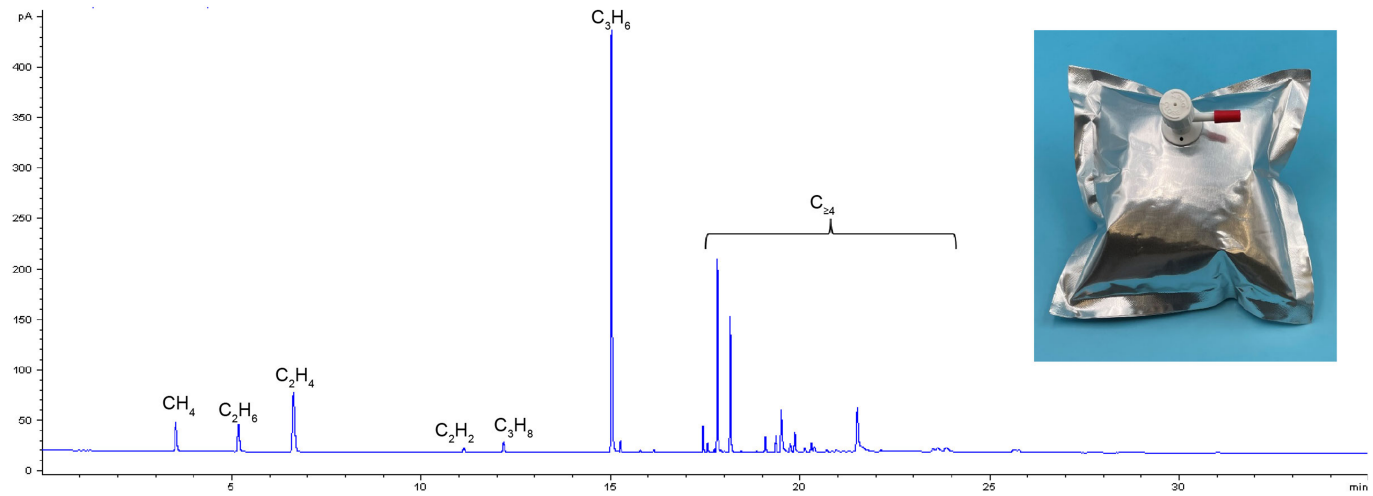

Extended Data Fig. 4 | A typical gas chromatograph of the PP pyrolysis products by STH (0.11 s power on at about 22 V and 0.99 s power off). Inset, the gas bag used to collect the reaction products in the gas phase, which is connected downstream in the STH system.

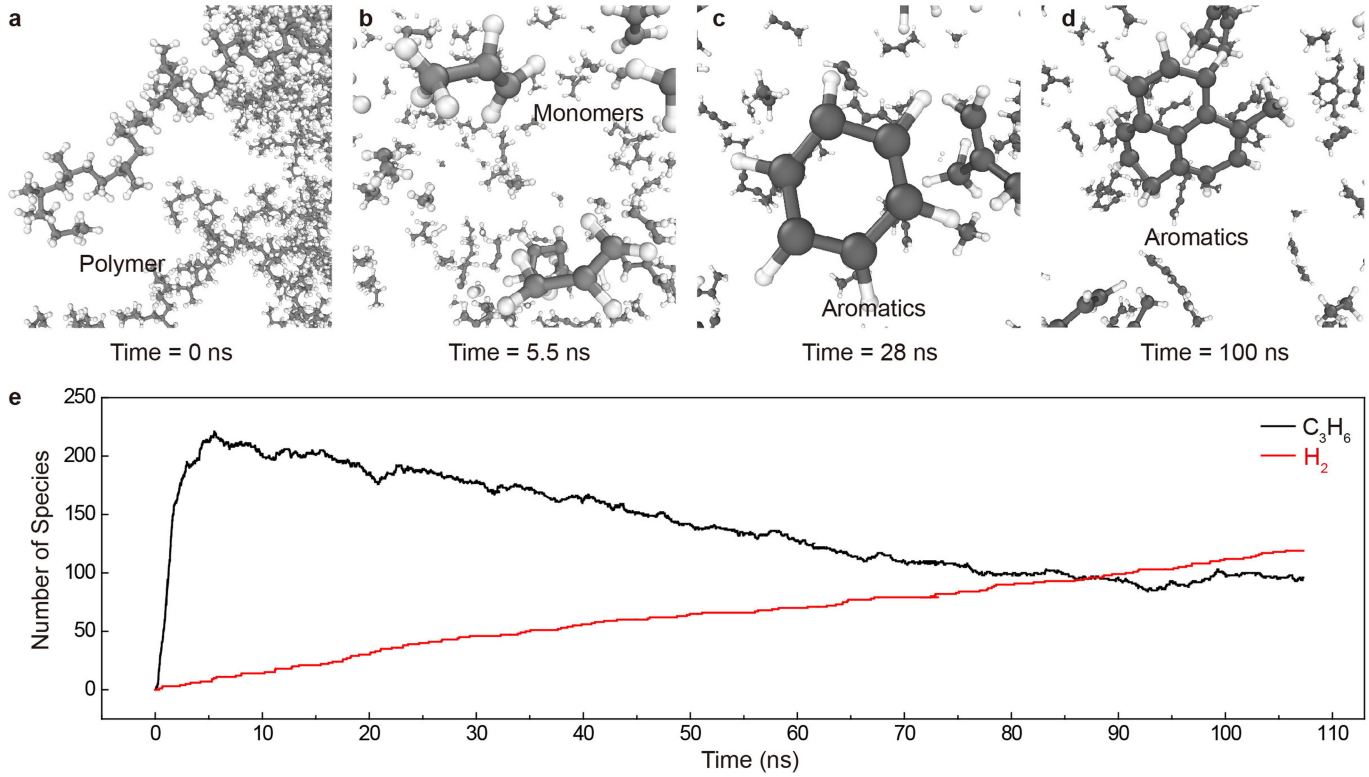

Extended Data Fig. 5 | Reactive molecular dynamics simulations of PP pyrolysis at 1,527 °C. a–**d**, A series of representative images of the simulated space, showing the transition from PP (0 ns; **a**) to a large number of C_3H_6 monomers (about 5.5 ns; **b**), and then to various aromatic species (about 28–100 ns; **c** and **d**) owing to dehydrogenation and aromatization under extended continuous heating. **e**, The counts of C_3H_6 and H_2 molecules throughout the simulated reaction time frame. The number of C_3H_6 monomers reaches a peak concentration within a short period of time (about 5.5 ns), followed by a gradual drop owing to dehydrogenation, C–C bond coupling, aromatization etc., whereas the number of H_2 molecules continues increasing as the reaction approaches chemical equilibrium.

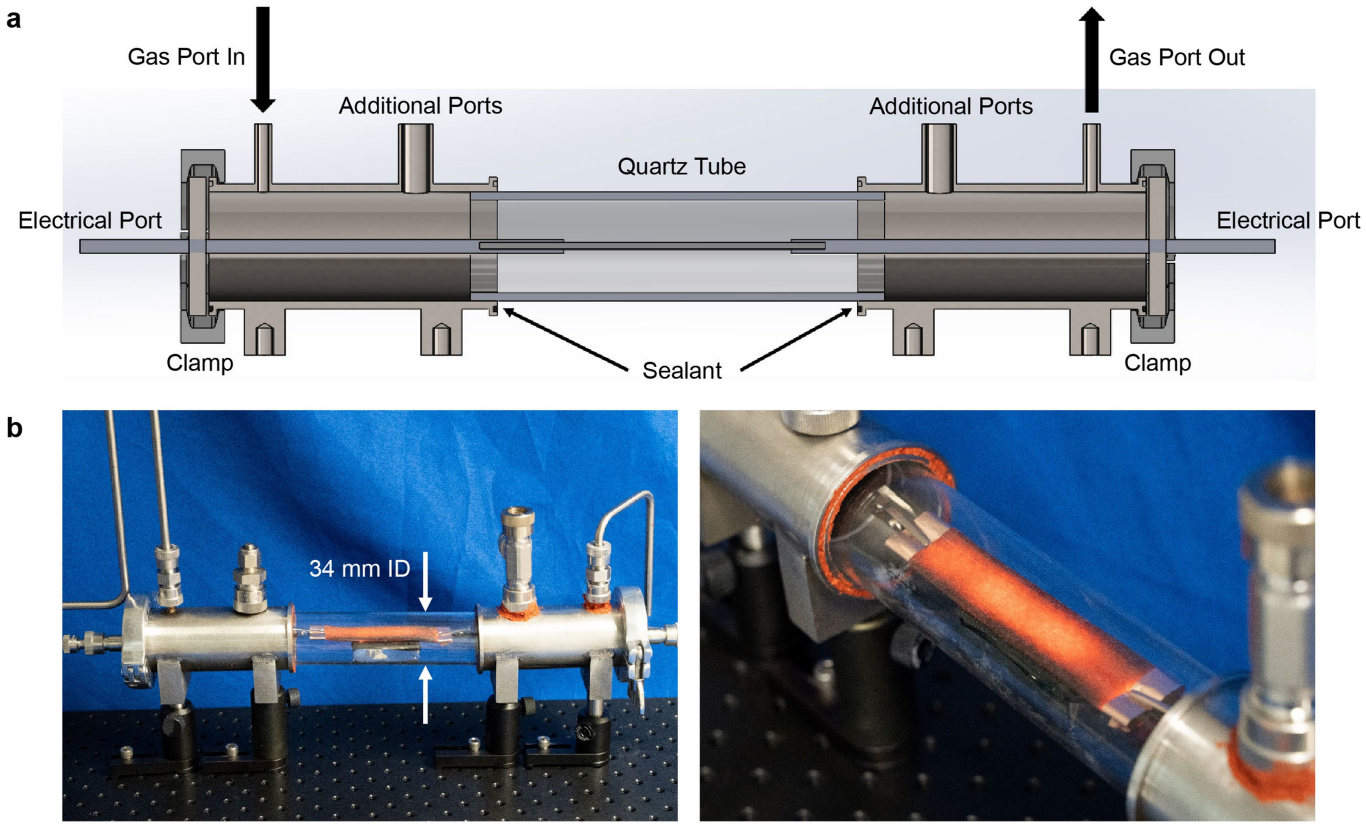

Extended Data Fig. 6 | The larger-scale STH system. Schematic (**a**) and images (**b**) of the larger-scale STH system. A quartz tube with 34 mm inner diameter was used to contain the carbon bilayer structure and reactant reservoir. This system allowed us to react up to 1.0 g of PP material within 35 min in a batch reaction mode.

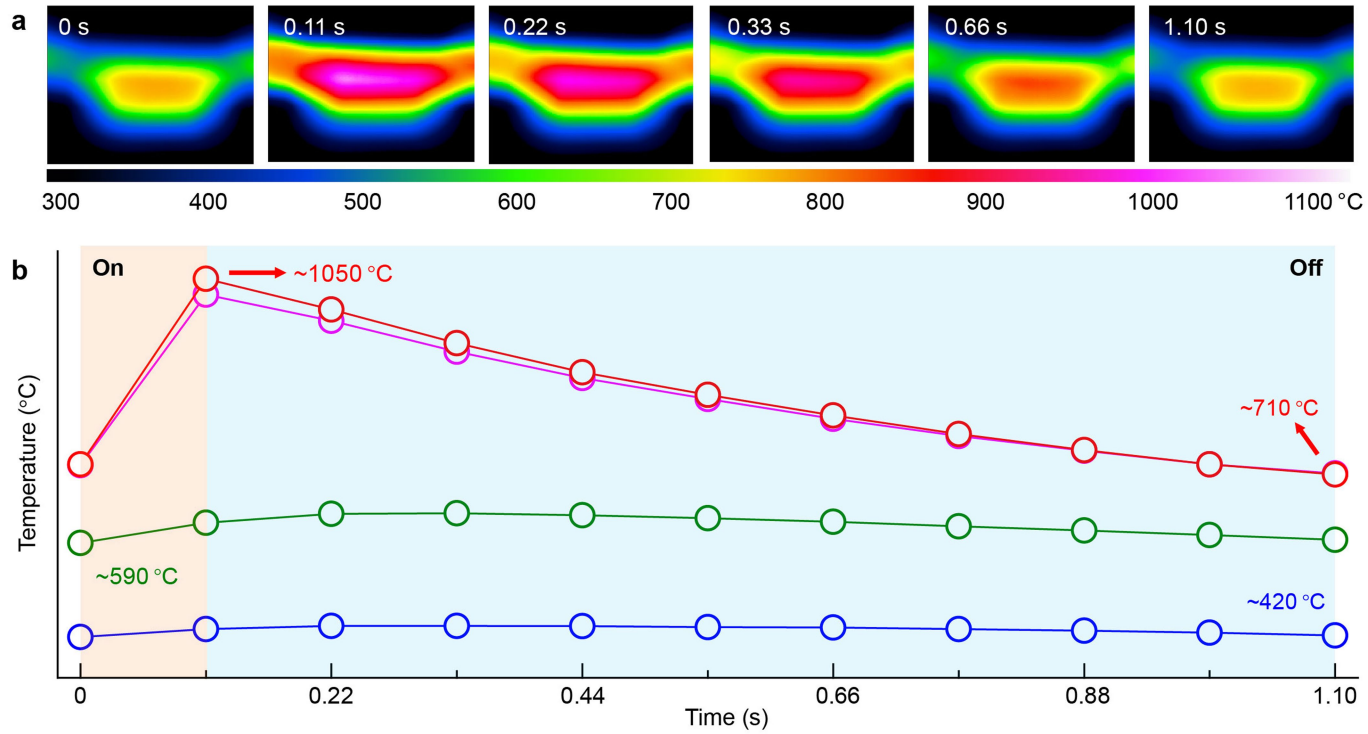

Extended Data Fig. 7 | Temperature measurement during the PET depolymerization by STH. a, Temperature maps of the heater and reactor layers at various time points during one heating cycle of 1.10 s (power on time: 0.11 s at about 26 V; power off time: 0.99 s). **b**, The temporal heating profiles of the four representative positions shown in Fig. 2c. The orange region indicates power on, whereas the blue region indicates power off.

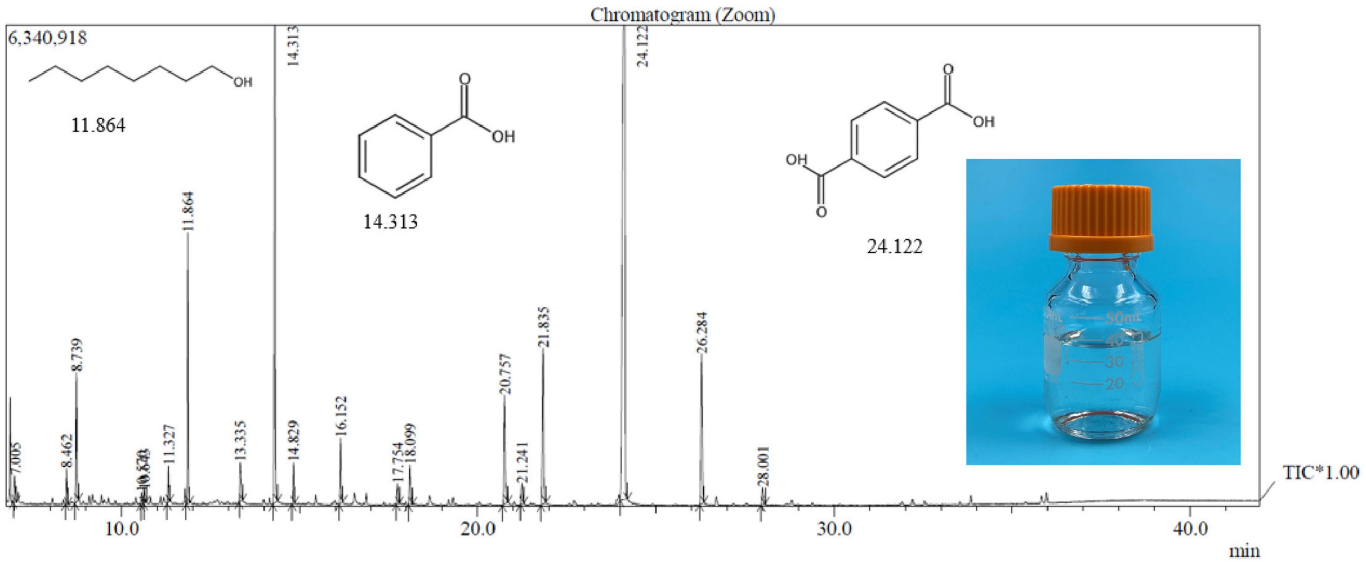

Extended Data Fig. 8 | Gas chromatograph by GC-MS of the liquid products from PET pyrolysis by means of STH using a heating duration of 0.11 s at about 26 V in a period of 1.10 s. Inset, digital image showing the collected products (about 2 wt% in acetone) after three batches of the STH process with PET. A fraction of the products was collected downstream with the carrier gas. The rest of the products condensed in the quartz tube, which was rinsed off using acetone and combined with the downstream products.

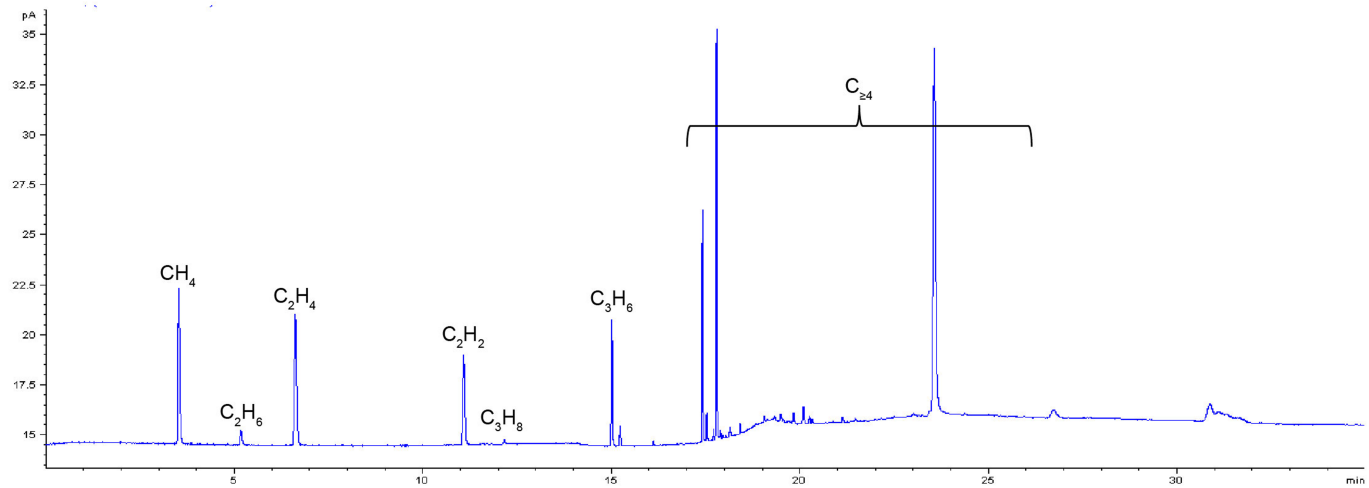

Extended Data Fig. 9 | A typical gas chromatograph by GC-FID of the gaseous products from the STH process with PET using a heating duration of 0.11 s at about 26 V in a period of 1.10 s. Acetylene is observed as one of the gaseous products, which is consistent with the β-CH hydrogen-transfer mechanism[35]. Note that acetylene is prone to secondary reactions, therefore the measured content does not directly reflect the total amount of acetylene produced along with the formation of 1,4-benzenedicarboxylic acid.

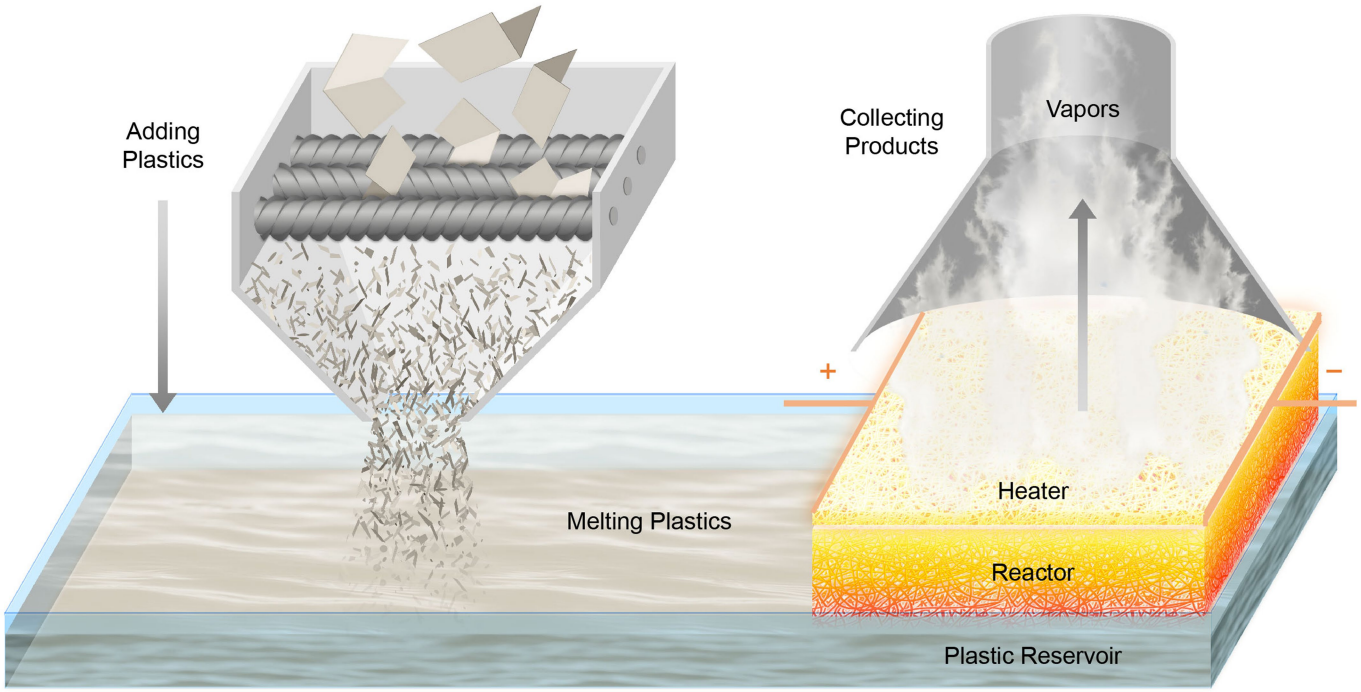

Extended Data Fig. 10 | A prototype design of a continuous STH process that involves melting, wicking, vaporization and reaction, along with pulsed electrical heating for recycling commodity plastics such as polyolefins and polyesters. The recycling system integrates commercially available tools and materials, demonstrating the potential practicality of the STH approach.